Langmuir
Article
pubs.acs.org/Langmuir
© 2010 American Chemical Society

Anisotropic Wetting on Microstrips Surface Fabricated by Femtosecond Laser

Feng Chen,*,† Dongshi Zhang,† Qing Yang,† Xianhua Wang,† Baojiang Dai,† Xiangming Li,‡ Xiuqing Hao,‡ Yucheng Ding,‡ Jinhai Si,† and Xun Hou†

†*Key Laboratory for Physical Electronics and Devices of the Ministry of Education & Shannxi Key Laboratory of Photonics Technology for Information, Xi'an Jiaotong University, 710049, China, and* ‡*State Key Laboratory for Manufacturing Systems Enginnering, Xi'an Jiaotong University, 710049, China*

Received August 18, 2010. Revised Manuscript Received October 27, 2010

In this paper, we present a new method to realize anisotropy by restricting a droplet on an unstructured Si hydrophobic domain between two superhydrophobic strips fabricated by femtosecond laser. The water contact angles and corresponding water baseline length were investigated. The results showed that anisotropy would vary with the volume-induced pinning−depinning−repinning behavior of the droplet. Furthermore, through the observation of water response on small Si domain, the adhesive force of the structure is proven to be the key factor giving rise to the anisotropy wetting. This phenomenon could potentially be used as a model for fundamental research, and such structures could be utilized to control large volume in microfluidic devices, lab-on-chip system, microreactors, and self-cleaning surfaces.

1. Introduction

Surface wettability, generally characterized by static contact angle (SCA) between a liquid droplet and a solid surface, is an important property of solid materials. A contact angle (CA) less than 90° is indicative of a hydrophilic surface, while CA greater than 90° is indicative of a hydrophobic surface. A surface with CA in excess of 150° and sliding angle (SA) less than 10° is defined as superhydrophobic.[1,2] If the contact angles (CAs) of a droplet placed on a surface are identical when measured from different directions, that is, the drop shape is spherical, the surface is said to be isotropic in wettability;[3−5] whereas the shape of a three-phase contact line and the drop appearance will be distorted under the influence of material chemical heterogeneity or heterogeneous topographic patterns, in which case the surface is defined as anisotropic.[6−8]

Nature has illustrated a wide variety of anisotropic surfaces. The rice leaf *Oryza sativa* has SA of 3−5° along the direction of the papilla but 9−15° perpendicular to the direction of the random distribution of micropapilla.[9] The faculty of water striders to glide on top of the water or move against the water by generating large propulsion forces is attributed to the SA anisotropy of groove-like structures on the hairs.[10] The directional arrangement of flexible nanotips on ridging nanostripes and microscales overlapping on the wings of the Morpho aega butterfly can produce different adhesive forces, so that a droplet could easily roll off the surface of the wings along the radial outward (RO) direction of the central axis of the body, but pin tightly against the RO direction.[11] The very small individual tooth-like scales of shark skin, ribbed with longitudinal grooves (aligned parallel to the local flow direction of the water), could result in water moving very efficiently over their surface.[12] Inspired from these fascinating features, controlled anisotropic wetting surfaces, on which droplets move spontaneously toward a preset route, have received significant attention for their potential applications in micropump needles, biochips, cell motility studies, directional water-collecting,[13] microfluidic devices,[14] evaporation-driven formation of patterns,[15] and drag-reduction coatings.[16] For example, Jacobi et al.[17,18] reported that drainage could be enhanced with the aid of wetting anisotropy on the aluminum surface through imparting parallel grooves. Higgins and Jones[19] realized anisotropic spinodal dewetting of a polymer surface simply by rubbing the substrate to give rise to patterns of remarkably well-aligned polymer lines. Philip Ball[20] reported that a transparent plastic film mimicking the same microscopic texture of shark skin could greatly reduce aircraft drag, thus leading its trial on aircraft coating.

*E-mail address: chenfeng@mail.xjtu.edu.cn.

(1) Li, X. M.; Reinhoudt, D.; Crego-Calama, M. *Chem. Soc. Rev.* **2007**, *36*, 1350–1368.
(2) Zhou, Y. B.; Yang, Y.; Liu, W. M.; Ye, Q.; He, B.; Zou, Y. S.; Wang, P. F.; Pan, X. J. *Appl. Phys. Lett.* **2010**, *97*, 133110.
(3) Shirtcliffe, N. J.; Aqil, S.; Evans, C.; McHale, G.; Newton, M. I.; Perry, C. C.; Roach, P. *J. Micromech. Microeng.* **2004**, *14*, 1384–1389.
(4) Chang, Y. C.; Mei, G. H.; Chang, T. W.; Wang, T. J.; Lin, D. Z.; Lee, C. K. *Nanotechnology* **2007**, *18*, 285303.
(5) Cao, L. L.; Hu, H. H.; Gao, D. *Langmuir* **2007**, *23*, 4310–4314.
(6) Wu, S. Z.; Wu, D.; Yao, J.; Chen, Q. D.; Wang, J. N.; Niu, L. G.; Fang, H. H.; Sun, H. B. *Langmuir* **2010**, *26*, 12012–12016.
(7) Bliznyuk, O.; Jansen, H. P.; Kooij, E. S.; Poelsema, B. *Langmuir* **2010**, *26*, 6328–6334.
(8) Zhang, F. X.; Low, H. Y. *Langmuir* **2007**, *23*, 7793–7798.
(9) Feng, L.; Li, S. H.; Li, Y. S.; Li, H. J.; Zhang, L. J.; Zhai, J.; Song, Y. L.; Liu, B. Q.; Jiang, L.; Zhu, D. B. *Adv. Mater.* **2002**, *14*, 1857–1860.
(10) Bush, J. W. M.; Hu, D. L.; Prakash, M. The Integument of Water-walking Arthropods: Form and Function. In Insect Mechanics and Control; Casas, J., Simpson, S. J., Eds.; *Advances in Insect Physiology*, Vol. *34*; Academic Press: New York, 2007; pp 117−192.
(11) Zheng, Y. M.; Gao, X. F.; Jiang, L. *Soft Matter* **2007**, *3*, 178–182.
(12) Bhushan, B. *Phil. Trans. R. Soc. A* **2009**, *367*, 1445–1486.
(13) Zheng, Y. M.; Bai, H.; Huang, Z. B.; Tian, X. L.; Nie, F. Q.; Zhao, Y.; Zhai, J.; Jiang, L. *Nature* **2010**, *463*, 640–643.
(14) Zhao, B.; Moore, J. S.; Beebe, D. J. *Science* **2001**, *291*, 1023–1026.
(15) Xia, D. Y.; Brueck, S. R. J. *Nano Lett.* **2008**, *8*, 2819–2824.
(16) Jung, Y. C.; Bhushan, B. *J. Phys.: Condens. Matter* **2010**, *22*, 035104.
(17) Sommers, A. D.; Jacobi, A. M. *J. Micromech. Microeng.* **2006**, *16*, 1571–1578.
(18) Liu, L. P.; Jacobi, A. M.; Chvedov, D. *J. Micromech. Microeng.* **2009**, *19*, 035026.
(19) Higgins, A. M.; Jones, R. A. L. *Nature* **2000**, *404*, 476–478.
(20) Ball, P. *Nature* **1999**, *400*, 507–509.

Due to their excellent performance and widespread use, anisotropic wetting surfaces have been obtained by either modifying rough micropatterns with materials of low surface energy or texturing geometrically anisotropic structures. Up to now, alternating microgrooves/microstrips are the most popular anisotropic geometries because of their ease of experimental manufacture and theoretical modeling. Zhao et al.[21] realized weak anisotropic wetting characteristics on submicrometer-scale (groove widths of 318, 396, and 513 nm with varying nanometer-scale depth) periodic grooved structures, and found that water CA measured from the direction perpendicular to the grooves increased with increasing groove depth, in accordance with the reports written by Wu et al.[22] and Xia et al.[23] who revealed that anisotropy would significantly increase from 9° to 48° with height varying from 100 nm to 1.3 μm or go up from 67° to 81° by raising the pitch height from 250 nm to 800 nm with a periodicity of 1000 nm, all of which confirmed the strong relationship between anisotropy and groove height. Besides these determinants, the period also has an influence on anisotropy, proven not only by the literature of Xia et al.[15] who indicated that anisotropy would tune from 61° to 79° with period ranging from 420 nm to 1500 nm for periodic nanoscale strips 500 nm in height, but also by the observational shape alteration of 2 μL drops on hydrophobic ridges of 5 μm in width and 5−20 μm at interval.[24] Further, the advancing θ_{adv} and receding θ_{rec} contact angles (CAs) were also investigated for their faculty for characterizing the minimum tilting angle of a surface at which a liquid droplet will spontaneously slide down.[25] For instance, Drelich et al.[26] pointed out θ_{adv} and θ_{rec} on chemically heterogeneous stripes of 2.5 μm thickness were 2−10° higher when viewing the drop parallel to the stripes rather than perpendicular to the stripes. Morita et al.[27] also reported the dynamic CAs, SCA, and SA on the line-patterned surface of a fluoroalkylsilane monolayer with strips ∼1−20 μm in width, exhibiting higher values than the previous reference. Bico et al.[28] obtained an anisotropy state with θ_{adv} and θ_{rec} of 18° and 7° on ridges 1 μm wide and 1 μm tall. An ∼30° higher θ_{adv} in the direction perpendicular to the ridges compared to that parallel to the ridges appeared on aluminum ridges of 30 μm in width.[17] In addition, Chen et al.[29] reported angular dependence of SCAs on hydrophobic ridges with stripe width of 23 μm, groove width of 25.6 μm, and groove depth of 30 μm, and pointed out that experimetally observed droplet geometry does not necessarily correspond to the lowest energy state. Yoshimitsu et al.[30] showed a better water-shedding property in the parallel vs perpendicular direction on the micropillar structure with pillar width, groove width, and pillar height of 96, 49, and 160 μm, respectively. Peter Lenz and Lipowsky[31] reported that the wetting layer may undergo morphological transitions among three different states as the water volume increases on the surface consisting of hydrophilic stripes and hydrophobic surface domains, and the morphologies have been observed experimentally.[32] They then investigated the interplay between the two-dimensional patterns of surface domains and theoretically studied the three-dimensional morphology of the wetting fluid.[33−36]

To date, the preparation of periodic grooves is often achieved by the use of complex, multistep patterning procedures, including interferometric lithography,[15] vacuum ultraviolet (VUV) photolithography,[27] and deep reactive ion etching combined with photolithography.[37] Nevertheless, these methods suffer from the shortcomings of high cost and indispensable masks, thereby resulting in their being unable to be applied to large-scale applications in industries. A femtosecond laser (fs) has been proven to be a powerful one-step production technology to realize complex surface topologies with two length scales due to the advantages of a negligible heat-affected zone, precise ablation threshold, and high resolution, without the need for a clean room facility and high-vacuum equipment. It has been utilized recently to develop superhydrophobic surfaces.[38−44] However, among these, there are few reports devoted to the anisotropy of structures patterned by femtosecond irradiation except our previous paper,[45] especially no deliberate effort to obtain anisotropy by confining a droplet between only two superhydrophobic parallel strips in the micrometer/millimeter scale to study the corresponding volume-induced behavior.

In the present paper, we reported that anisotropy could be achieved simply by restricting a water droplet on a hydrophobic Si surface domain between two superhydrophobic strips developed by femtosecond laser micropatterning. The relationships among CAs, water baseline, and drop volume were investigated, and the results showed that anisotropy would increase with increasing droplet volume but dramatically decrease in the case of drop collapse. We interpreted such anisotropy with a maximal value of 40° and droplet distortion as a consequence of energy barrier difference from two orthogonal directions and contact line pinning. The structure could find many potential applications in microfluidic devices, lab-on-chip systems, microreactors, and self-cleaning surfaces. The videos of the phenomenon mentioned above can be downloaded from the Supporting Information.

2. Experimental Section

2.1. Material. We used n-doped Si (100) wafers. After structuring the silicon substrates in air atmosphere by femtosecond laser irradiation, the samples were cleaned by ultrasonic cleaning in water at 40° for 15 min, and then by a 15 min ultrasonic bath in acetone and in methanol in sequence. Immediately afterward, the

(21) Zhao, Y.; Lu, Q. H.; Li, M.; Li, X. *Langmuir* **2007**, *23*, 6212–6217.
(22) Wu, D.; Chen, Q. D.; Yao, J.; Guan, Y. C.; Wang, J. N.; Niu, L. G.; Fang, H. H.; Sun, H. B. *Appl. Phys. Lett*. **2010**, *96*, 053704.
(23) Xia, D. Y.; He, X.; Jiang, Y. B.; Lopez, G. P.; Brueck, S. R. J. *Langmuir* **2010**, *26*, 2700–2706.
(24) Carman, M. L.; Estes, T. G.; Feinberg, A. W.; Schumacher, J. F.; Wilkerson, W.; Wilson, L. H.; Callow, M. E.; Callow, J. A.; Brennan, A. B. *Biofouling* **2006**, *22*, 11–21.
(25) Yeh, K. Y.; Chen, L. J.; Chang, J. Y. *Langmuir* **2008**, *24*, 245–251.
(26) Drelich, J.; Wilbur, J. L.; Miller, J. D.; Whitesides, G. M. *Langmuir* **1996**, *12*, 1913–1922.
(27) Morita, M.; Koga, T.; Otsuka, H.; Takahara, A. *Langmuir* **2005**, *21*, 911–918.
(28) Bico, J.; Marzolin, C.; Quere, D. *Europhys. Lett*. **1999**, *47*, 220–226.
(29) Chen, Y.; He, B.; Lee, J.; Patankar, N. A. *J. Colloid Interface Sci*. **2005**, *281*, 458–464.
(30) Yoshimitsu, Z.; Nakajima, A.; Watanabe, T.; Hashimoto, K. *Langmuir* **2002**, *18*, 5818–5822.
(31) Lenz, P.; Lipowsky, R. *Phys. Rev. Lett*. **1998**, *80*, 1920–1923.
(32) Gau, H.; Herminghaus, S.; Lenz, P.; Lipowsky, R. *Science* **1999**, *83*, 46–49.
(33) Lenz, P. *Adv. Mater*. **1999**, *11*, 1531–1534.
(34) Lenz, P.; Lipowsky, R. *Eur. Phys. J. E* **2000**, *1*, 249–262.
(35) Lipowsky, R.; Lenz, P.; Swain., P. S. *Colloids Surf., A* **2000**, *161*, 3–22.
(36) Lipowsky, R. *Curr. Opin. Colloid Interface Sci*. **2001**, *6*, 40–48.
(37) Long, C. J.; Schumacher, J. F.; Brennan, A. B. *Langmuir* **2009**, *25*, 12982–12989.
(38) Baldacchini, T.; Carey, J. E.; Zhou, M.; Mazur, E. *Langmuir* **2006**, *22*, 4917–4919.
(39) Zorba, V.; Persano, L.; Pisignano, D.; Athanassiou, A.; Stratakis, E.; Cingolani, R.; Tzanetakis, P.; Fotakis, C. *Nanotechnology* **2006**, *17*, 3234–3238.
(40) Zorba, V.; Stratakis, E.; Barberoglou, M.; Spanakis, E.; Tzanetakis, P.; Fotakis, C. *Appl. Phys. A: Mater. Sci. Process*. **2008**, *93*, 819–825.
(41) Wang, Z. K.; Zheng, H. Y.; Lim, C. P.; Lam, Y. C. *Appl. Phys. Lett*. **2009**, *95*, 111110.
(42) Kietzig, A. M.; Hatzikiriakos, S. G.; Englezos, P. *Langmuir* **2009**, *25*, 4821–4827.
(43) Wu, B.; Zhou, M.; Li, J.; Ye, X.; Li, G.; Cai, L. *Appl. Surf. Sci*. **2009**, *256*, 61–66.
(44) Yoon, T. O.; Shin, H. J.; Jeoung, S. C.; Park, Y. I. *Opt. Express* **2008**, *16*, 12715–12725.
(45) Zhang, D. S.; Chen, F.; Fang, G. P.; Yang, Q.; Xie, D. G.; Qiao, G. J.; Li, W.; Si, J. H.; Hou, X. *J. Micromech. Microeng*. **2010**, *20*, 075029.

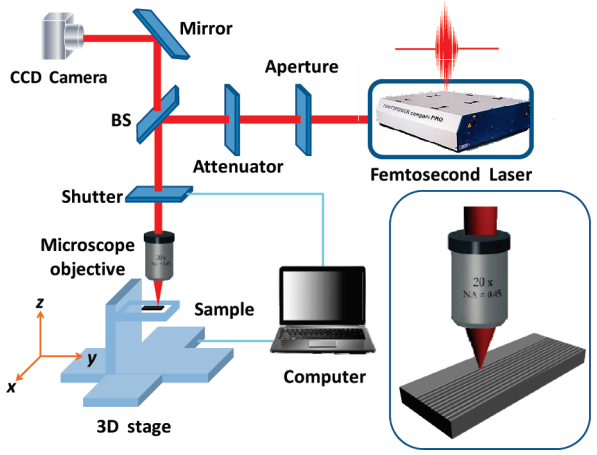

Figure 1. Schematic of experimental setup.

samples were immersed into fluoroalkylsilane solution with a concentration of 2% for two hours and then were roasted in a furnace with temperature constant of 300 °C for another 12 h.

2.2. Surface Laser Irradiation. The schematic of experimental setup is shown in Figure 1. A Ti:sapphire laser system (Femtopower compact Pro) with a pulse width of 30 fs at a fundamental wavelength 800 nm and a repetition rate of 1 kHz was used. The beam mode and pulse energy were, respectively, adjusted by a variable aperture and a neutral density (ND) attenuator. A mechanical shutter was utilized to turn the laser beam on and off. The laser beam was subsequently focused with a microscope objective lens (20×, NA = 0.45, Nikon) into the sample (dimensions 5 × 5 × 0.5 mm^3) which was mounted on a precision computer-controlled $x-y-z$ translation stage with step resolution of 50 nm and a maximum speed of 3 mm/s. Each sample was fabricated with constant average power of 13 mW at scanning speed of 1 mm/s, in which case the laser spot size is 12 μm. The interval of adjacent laser scanning lines was held constant at 2 μm.

2.3. Surface Analysis. The morphology of the surface structures was analyzed with a scanning electron microscopy (SEM) and an optical microscope (LV100D, Nikon).

2.4. Contact Angle Characterization. CA characterization was performed using a Dataphysics OCA20 CA goniometer with an automated drop dispenser and image and video capture system. The digital drop images were processed by the image analysis system, which calculated both the left and right CAs from the drop shape with an accuracy of ±0.1°. SCA images were captured by the video recorded before the first drop was extruded from the drop dispenser, and ended after the droplet collapsed. Each increasing amount of deionized water dispensed on the sample surface was 0.5 μL with the volume speed of 0.5 μL/s. The reported CAs and water morphologies are supported by the videos in the Supporting Information. The camera for recorded images of drops worked at a speed of 23 fps.

2.5. Contact Angle Measurements. With respect to $\theta > 90°$, for the small water volume, the contact angle is assumed to form a spherical cap[46] and is calculated as shown in Figure 2a, where R is the radius of curvature of the drop, d is its diameter, and θ is the mean contact angle. However, if a drop is so large it would be flattened to some extent, in which case the result from spherical cap algorithm θ_1 would not be applicable,[47] smaller than the value θ_2 obtained by the tangent algorithm in OCA20 software, as shown in Figure 2b. The experimental measurement results are shown in Supporting Information Figure S1. The diameter d here is defined as the baseline (BL) for the droplet distortion, measured through the images of droplet morphologies captured by videos.

(46) Zhang, J.; Gao, X. F.; Jiang, L. *Langmuir* **2007**, *23*, 3230–3235.
(47) Sheng, X. L.; Zhang, J. H.; Jiang, L. *Langmuir* **2009**, *25*, 9903–9907.

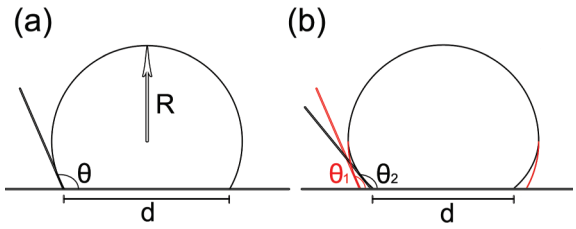

Figure 2. (a) Contact angle θ measurement using the spherical cap algorithm in the case of no water distortion. (b) Contact angles measured using different methods under the condition of water deformation. θ_1 and θ_2, respectively, correspond to the spherical cap algorithm and the tangent algorithm.

Results and Discussion

Morphology and Wetting Characteristics of Structured Surface. Figure 3g shows the schematic illustration elucidating the basic principle of anisotropy constrained by two femtosecond etching parallel stripes (Figure 3a), characterized by tens or a few hundreds of nanometer-sized protrusions decorating the self-organized conical spike forests with 10 μm in width and period of 10 μm (Figure 3b–f). Such a structure is considered to be the micrometer-scale ridges on top of the ripples as an adjacent scanning line passed by.[48,49] The constant density and spacing of the spikes is attributed to the fixed values of scanning velocity and laser power. The CAs measured from the directions orthogonal to and parallel to the parallel strips (PS) are, respectively, defined as $\theta_\perp$ and $\theta_\parallel$. The static and dynamic wettability of the spikes is shown in Figure 4. First, an 8 μL water droplet was suspended on a microsyringe (Figure 4a) and then tightly contacted the lifted sample consisting of spikes (Figure 4b). It is found that the suspending droplet had difficulty falling on the structured surface; that is, in comparison to the large droplet, the surface adhesion was negligible even though the droplet was deformed severely (Figure 4c) by the upward pushing force produced during sample elevation, thus making the drop depart easily from the gradually lowering surface without any droplet remaining (Figure 4d). The apparent CA should be considered to be close to 180° due to the invalidity of the conventional sessile droplet method.[50] However, as water dosage reached 9.0 μL, the droplet separated from the microsyringe by the adhesive force of the structure and then fell on the 2.5° tilted sample and instantaneously rolled off under the gravitation effect (Figure 4e). All these substantiate the superhydrophobic properties of the periodic spikes.

Anisotropy Dependence on Strip Width. Figure 5 shows anisotropic images of 0.5 μL, 1.0 μL, and 1.5 μL water droplets on a 500-μm-wide hydrophobic Si domain with strip width (SW) of 200 μm (see Supporting Information movies S3, S4). Surprisingly, it is observed that the first 0.5 μL droplet was instantaneously constrained between two strips edges (SE) once the liquid came in contact with the Si domain between two structured strips. The drop was still suspended when the drop volume reached 1 μL, characterized by $\theta_\parallel$ slightly decreasing by 1° and $\theta_\perp$ increasing by 2° (Figure 5g), but it came down in the case of the third 0.5 μL water addition, as demonstrated in Figure 5c and f. Meanwhile, the water collapse resulted in a sharp decrease in $\theta_\parallel$ coupled with a small increase in $\theta_\perp$, thus directly leading to the anisotropy transition of $\theta_\perp$ larger than $\theta_\parallel$, which could be speculated from

(48) Her, T. H.; Finlay, R. J.; Wu, C.; Deliwala, S.; Mazur, E. *Appl. Phys. Lett.* **1998**, *73*, 1673–1675.
(49) Shen, M. Y.; Crouch, C. H.; Carey, J. E.; Mazur, E. *Appl. Phys. Lett.* **2004**, *85*, 5694–5696.
(50) Gao, X. F.; Yao, X.; Jiang, L. *Langmuir* **2007**, *23*, 4886–4891.

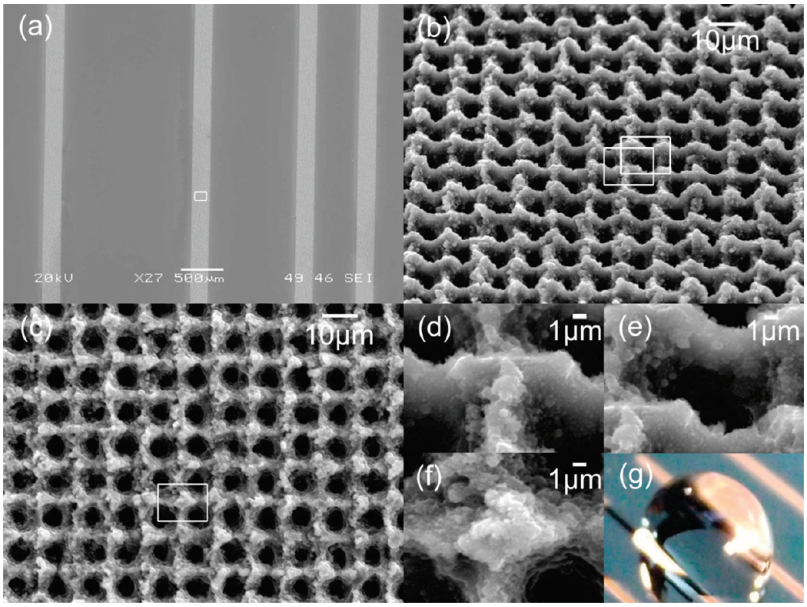

Figure 3. (a) SEM image of parallel strips achieved by femtosecond laser irradiation on silicon wafers, with Si strip domain width ranging from 500 to 1500 μm and strip width of 200 μm. (b,c) 45° tilted view and top view SEM images of microstructures on strips. (d−f) Corresponding magnification SEM images. (g) Optical image of water drop restricted by two strips.

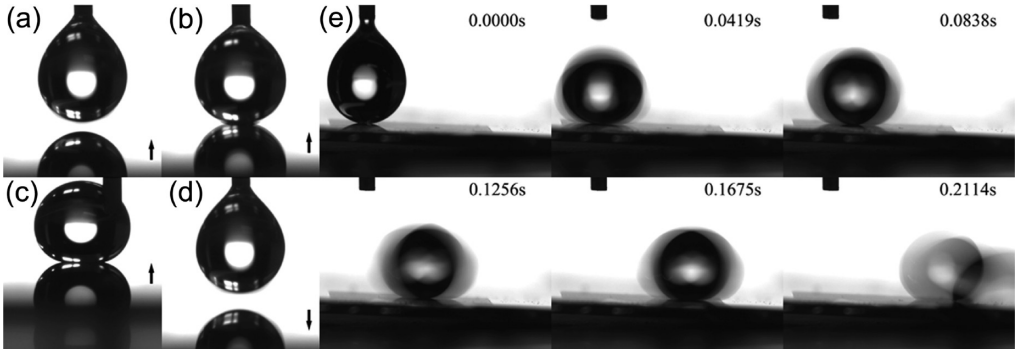

Figure 4. (a−d) Water images during SCA measurements of the periodic spikes without strips: 8 μL water droplet (a) suspended on a microsyringe; (b) tightly contacted with the lifting surface; (c) distorted by water due to the increasing upward pushing force; (d) departed from the lowering surface. (e) 9 μL water of drop, which fell on a 2.5° tilted surface and instantaneously rolled off. In the top right of each image is the time sequence.

the comparison of BL length in the orthogonal directions with $BL_\perp$ less than $BL_\parallel$. The similar phenomenon of $\theta_\perp$ larger than $\theta_\parallel$ has been observed and simulated using the Lattice Boltzmann equation by Kusumaatmaja[51] who attributed this to smaller receding angle in the perpendicular direction than that parallel to the strips. Nevertheless, the receding motion he focused on differs from the spreading process because of the breakdown of the water droplet we present here. The reason for this phenomenon can be envisaged to follow the principle in which the droplet spread out much further after it broke through the energy barrier exerted by the strips, while the droplet spread a little perpendicular to strips due to the pinning of periodic spikes, thus leading to the final shape elongation perpendicular to the strips.

To gain further insight into the relationships between droplet volume and CAs as well as matching water baseline, experiments were performed with Si domain width (SDW) ranging from 1 mm to 2.5 mm stepwise by 0.5 mm with SW constant equal to 200 μm. The results are shown in Figure 6. For SDW varying from 1.5 mm to 2.5 mm, no pinning happened due to BL being less than SDW when the first 0.5 μL water was gently placed on the flat Si pillar between two strips, as demonstrated by the images in Figure 6b−d with smallest water volume. At the first stage of the water dose increment, the plots for different SDW almost overlap with $\theta_\parallel$ almost equivalent to $\theta_\perp$ and both slightly decreasing because of the lack of water distortion, except in the case of SDW = 1 mm where $\theta_\parallel$ is larger than $\theta_\perp$ and both increase with increasing water volume. $BL_\parallel$ is 912 μm for SDW = 1 mm, which is smaller than the baseline diameter, 970 μm, of 0.5 μL water on the Si domain; meanwhile, $BL_\perp$ is 1000 μm. The small spreading discrepancy in different directions confirmed that the water pinning was just generated from the beginning, thus leading to the CA distinction. The CA separation points (Figure 6b−d) indicate the dosage beyond which water reached the edges of the strips and the pinning of the water contact line started to take effect. In other words, at this time, $BL_\perp$ was approximately equal to or slightly higher than SDW of 1, 1.5, 2, and 2.5 mm, corresponding to a water volume of 0.5, 1.5, 4, and 7 μL, as shown by the second-row images in Figure 6; whereas $\theta_\parallel$ increased up to a value between 140° and 155° for different SDW, while $\theta_\perp$

(51) Kusumaatmaja, H.; Vrancken, R. J.; Bastiaansen, C. W. M.; Yeomans, J. M. *Langmuir* **2008**, *24*, 7299–7308.

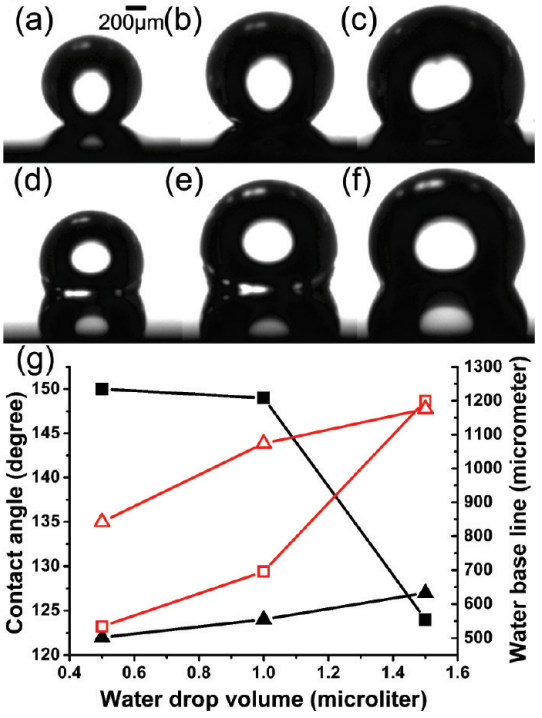

Figure 5. (a−f) Anisotropic images of 0.5 μL, 1 μL, and 1.5 μL water droplets on the 500-μm-wide hydrophobic domain between two periodic strips 200 μm in width: (a−c) images captured parallel to PS; (d−f) images captured orthogonal to PS. (g) Contact angles and water baseline vs water drop volume. (■) $\theta_{\parallel}$; (▲) $\theta_{\perp}$; (□) $BL_{\parallel}$; (△) $BL_{\perp}$.

hardly changed, stabilizing at around 110°, thus leading to the maximal anisotropy of 40° appearing at SDW = 2.5 mm. As the drop volume increased, the cumulative droplet would finally give way and stop at the adjacent strip's edge (SDW = 0.5, 1 mm) or reach an equilibrium shape on the Si surface (SDW = 1.5, 2, 2.5 mm), characterized by $BL_{\parallel}$ increasing significantly but $BL_{\perp}$ increasing only a little, directly leading up to the sharp descrease in $\theta_{\parallel}$. Note that $\theta_{\perp}$ hardly changed for SDW = 1 mm, but decreased by degrees as SDW increased as a result of the larger $BL_{\parallel}$ spreading range. The volume of water needed to break through the strip barrier rose with increasing SDW corresponding to 1.5, 5, 9.5, 24.5, and 43 μL for SDW = 0.5, 1, 1.5, 2, and 2.5 mm. The small deviations between $\theta_{\perp}$ and $\theta_{\parallel}$ on the Si domain where no pinning occurred, as shown in Figure 6, may be due to the heterogeneity of the Si substrate.

Response on Smaller Pillar Width. SDW of 200 μm was employed to compare the results of droplets landing on larger SDW as mentioned before. Figure 7 shows a selected time sequence of snapshots showing a 0.5 μL water drop tending to stay on a 200-μm-wide pillar gently and forcibly (Supporting Information movie S5). As shown in Figure 7a, when the drop gently contacted the pillar, the droplet seemed to be squeezed by both sides of the strips, distinguished by the air glistening beneath the drop, and further confirmed by the air bladder between the droplet and the solid surface during the lifting process in Figure 7b. Eventually, the drop finally broke into two parts with the small one attaching to the pillar and larger part hanging up on the microsyringe, distinct from the ordinary results with the whole droplet being totally lifted up[50] or adhering to surfaces,[45] thus giving evidence of the existence of an adhesion force and pinning.

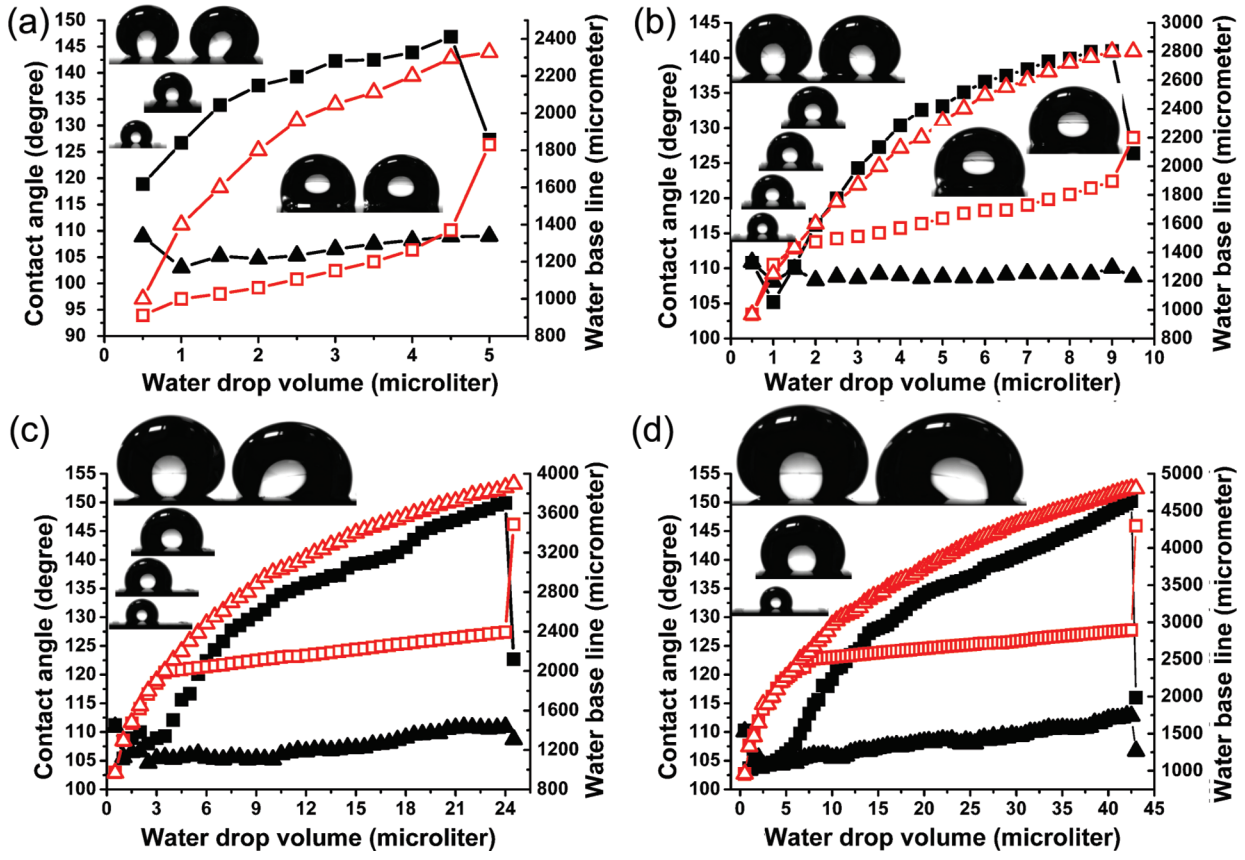

Figure 6. (a−d) Water contact angle and water baseline vs water drop volume on 1 mm, 1.5 mm, 2 mm, and 2.5 mm wide Si domain between two periodic spike strips of 200 μm in width. (■) $\theta_{\parallel}$; (▲) $\theta_{\perp}$; (□) $BL_{\parallel}$; (△) $BL_{\perp}$.

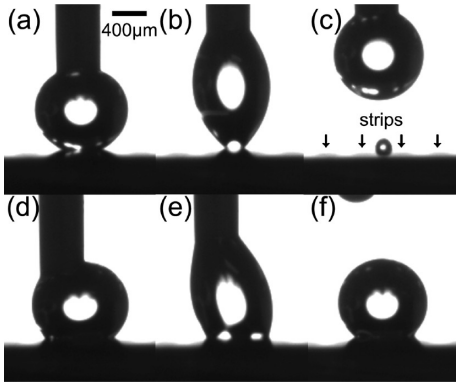

Figure 7. Selected snapshots of a 0.5 μL water droplet tending to land on the 200-μm-wide pillar between two 200 μm strips. (a−c) and (d−f) are the images of water being gently or forcibly put on the pillar and subsequently lifted up.

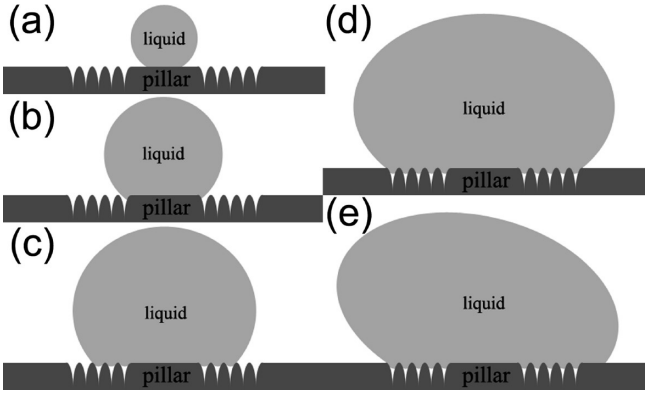

Figure 8. Schematic representation of macroscopic wetting anisotropy.

It can be deduced from the phenomenon that, for the pillar between two superhydrophobic strips, there exists a critical drop volume value, below which the drop will tend to land on the pillar intermediate or it would come down and spread outward, as Figure 7d−f indicates. However, SDW should be larger than 0.1 μm, the critical value for generating anisotropy predicted by Morita et al.[27] In comparison, the water no longer broke apart but all adhered to the surface. This fits with the well-known anisotropy generated by instantaneous spreading of water resulting from the considerable droplet weight and larger baseline compared to SDW, accordingly lending credence to the importance of the adhesive force of structures in giving rise to anisotropy.

Potential Mechanism Analysis. The Wenzel[52] or Cassie−Baxter[53] models are insufficient to explain anisotropy because they do not take into account the pinning effect of surface patterns, which has the ability to restrict water flow by circular strips of different height and slope[47,54] or hold liquid with the sample turning upside down.[55−59] The mechanism of a similar phenomenon has been reported in the literature,[31] which investigated the morphological transitions on the surface consisting of parallel hydrophilic stripes and hydrophobic surface domains, defined as γ and β surface, respectively. The whole water volume-induced process is distinguished into three different regimes by the critical droplet volume $V_d(R, \theta)$, where R is the radius of the shape of a cylindrical segment and θ is the contact angle. (i) Regime 1: for $V < V_d(R, \theta_\gamma)$, the droplet wets only part of the hydrophilic domain; (ii) for $V_d(R, \theta_\gamma) \le V \le V_d(R, \theta_\beta)$, the droplet covers the hydrophilic domain completely and the contact area is fixed; (iii) for $V > V_d(R, \theta_\beta)$, the contact area exceeds the area of the hydrophilic domain and comes in contact with the hydrophobic area, then increases with V. This process was supported by experimental observation and theoretical calculation; in the case of liquid channels, the homogeneous state with a spatially constant cross section undergoes a shape instability to a state with a single bulge when the liquid volume reaches a critical value.[33] On the basis of their explanation, we propose that the mechanism of macroscopic-wetting anisotropy follows the trend, as illustrated in Figure 6. There should be two critical values of water volume because of two interfaces: one is hydrophobic Si and superhydrophobic spikes at the beginning; the other is the value beyond which water breaks into the adjacent Si domain, defined as V_1 and V_2 respectively. When $V < V_1$, the drop only wets the Si domain; in other words, SDW is larger than the drop BL, and the droplet could not reach SE leading to CAs equal to the intrinsic CAs of the flat Si surface (Figure 8a). As the drop volume increases, the contact area increases, and when $V = V_1$, the drop reaches SE and covers the Si domain completely (Figure 8b), beyond which the drop is set back by the patterned structures of the strips, thus resulting in the preferential spreading parallel to the strips and the discrepancy between $\theta_\parallel$ and $\theta_\perp$, usually $\theta_\parallel$ larger than $\theta_\perp$. Qualitatively, the pinned contact line is believed to spread as the water volume increases (Figure 8c) until it arrives at a critical value V_2 near the outer edge (Figure 8d). At this time, the drop is so unstable that addition of extra small volume will lead the droplet across the final energy barrier of the stripe and advance with big strides until it attaches to another strip or reaches an equivalent state on the flat Si surface (Figure 8e). In the whole process, the droplet behaves in a pinning−depinning−repinning manner. It can be deduced that the adhesive force of the structure composed of nanoparticle and microprojection (Figure 3b−f) is the key factor for generating droplet distortion, acting as a "buffer zone" to slow down the water spreading perpendicular to the strips.

Conclusions

In summary, anisotropy was reported by restricting a droplet on a flat hydrophobic pillar between two superhydrophobic strips fabricated by one-step micromachining technology of a femtosecond laser irradiating on the Si surface, thus offering a high-speed and high-efficiency way to obtain a large-scale anistropic surface. The results showed that, as for a certain wide pillar, anisotropy was first generated in the case of water $BL_\parallel$ larger than the SDW, then subsequently enhanced with increasing droplet volume, and finally sharply decreased on the condition that the drop broke through the energy barrier of strips and instantaneously collapsed. Meanwhile, through the comparison of the results of 0.5 μL water drops on the 200 μm SDW surface gently and forcefully, the adhesive force of the structure is confirmed to play an important role in giving rise to anisotropy. We hope that the phenomenon would provide the potential model for fundamental research and femtoseond

(52) Wenzel, R. N. *Ind. Eng. Chem.* **1936**, *28*, 988–994.
(53) Cassie, A. B. D.; Baxter, S. *Trans. Faraday Soc.* **1944**, *40*, 546–551.
(54) Kalinin, Y. V.; Berejnov, V.; Thorne, R. E. *Langmuir* **2009**, *25*, 5391–5397.
(55) Li, Y. B.; Zheng, M. J.; Ma, L.; Zhong, M.; Shen, W. Z. *Inorg. Chem.* **2008**, *47*, 3140–3143.
(56) Huang, X. J.; Kim, D. H.; Im, M.; Lee, J. H.; Yoon, J. B.; Choi, Y. K. *Small* **2009**, *5*, 90–94.
(57) Jin, M. H.; Feng, X. J.; Feng, L.; Sun, T. L.; Zhai, J.; Li, T. J.; Jiang, L. *Adv. Mater.* **2005**, *17*, 1977–1981.
(58) Guo, Z. G.; Liu, W. M. *Appl. Phys. Lett.* **2007**, *90*, 223111.
(59) Cheng, Z. J.; Gao, J.; Jiang, L. *Langmuir* **2010**, *26*, 8233–8238.

laser micromachining would also provide a new way to produce anisotropic surfaces.

Acknowledgment. The authors gratefully acknowledge the financial support for this work provided by the National Science Foundation of China under the grant nos. 60678011 and 10674107 and National High Technology R&D Program of China under the grant no. 2009AA04Z305.

Supporting Information Available: Figure S1; Movies S1−5. This material is available free of charge via the Internet at http://pubs.acs.org.